Orange reflection from a three-dimensional photonic crystal in the scales of the weevil *Pachyrrhynchus congestus pavonius* (Curculionidae)

Victoria Welch,[1,2] Virginie Lousse,[1,3] Olivier Deparis,[1] Andrew Parker,[4] and Jean Pol Vigneron[1,*]

[1] *Laboratoire de Physique du Solide, Facultés Universitaires Notre-Dame de la Paix, 61 rue de Bruxelles, B-5000 Namur Belgium*
[2] *Department of Zoology, University of Oxford, South Park Road, Oxford, OX1 3PS, UK*
[3] *Ginzton Laboratory, Stanford University, Stanford, California 94305 USA*
[4] *Department of Zoology, The Natural History Museum, Cromwell Road, London, SW7 5BD, UK*

(Dated: January 22, 2007)

The three-dimensional structure which causes the colouration of the tropical weevil *Pachyrrhynchus congestus pavonius* was studied, using a combination of electron microscopy, optical spectroscopy and numerical modelling. The orange scales which cover the coloured rings on the animal's body were opened to display the structure of the selective reflection optical filter. This structure is a three-dimensional photonic crystal with a face-centred cubic symmetry. The measured lattice parameter and the observed filling fraction of this structure explains the dominant reflected wavelength in the reddish orange. Some long-range disorder in the form of a polycrystalline structure is also observed, explaining the paradoxical observation that the reflectance, though generated by a photonic-crystal, is insensitive to changes in the viewing angle.

PACS numbers: 42.66.-p, 42.70.Qs, 42.81.Qb

I. INTRODUCTION

Weevils are a group of beetles which are feared and famed in equal measure for the devastation some species can inflict on agricultural production, horticulture and on human food-stores, such as grain-barns. There are thought to be in the region of 40,000 species of weevil and both larvae and adults feed -variously- on the leaves, roots or fruits of specific plants, with a huge array of plants targeted between the different weevil species. There is, consequently, a large literature on this aspect of their biology.

The genus *Pachyrrhynchus* (also known as *"Pachyrhynchus"*), however, has never been associated with any adverse effect on crop-plants nor habitat destruction; instead, this group of approximately 100 weevil species, is known for its striking colouration, which Alfred Russel Wallace described as "surpass(ing) anything found in the whole Eastern hemisphere, if not in the whole world"! (see p 103 of ref. [1]).

The weevil which is investigated in this work is *Pachyrrhynchus congestus pavonius* (Heller 1921) - an insect found on Luzon, the largest island of the Philippine archipelago. *Pachyrrhynchus congestus pavonius* is shown in Fig. 1. The body and legs are dark and glossy, except for orange annular rings, which are flecked with marginal blue and green scales.

Our interest here is specifically in the orange part of the annular spots. Orange structural colouration is not very common in insects; on the other hand, it is known that the bright coloration of some weevils is caused by the presence of a three-dimensional structure. This structure can be opal-like (built from tiny chitin spheres [2]); observations of other species suggest an inverse opal, as can be found in Berthier (see p. 158 of ref. [3], also see refs. [4–6]). The precise objective of this work is to build upon these observations by elucidating the precise geometry of the colour-producing structure in the scales of this (previously unexamined) weevil species and relating it to its measured optical properties, using a combination of electron microscopy, optical spectroscopy and numerical modelling.

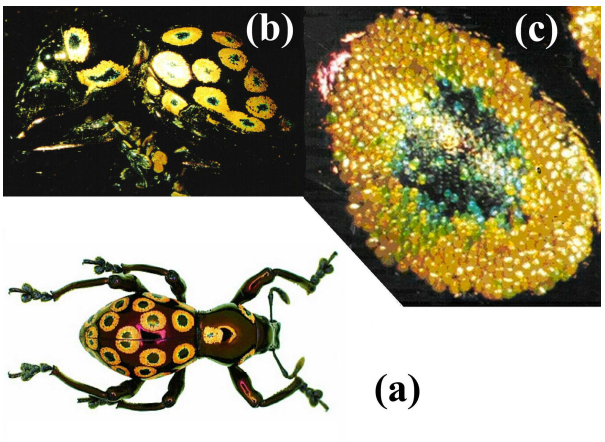

FIG. 1: (Colour online) *Pachyrrhynchus congestus pavonius* is a darkly coloured weevil, bearing highly conspicuous annular spots on the dorsal and lateral sides of its thorax and abdomen. (a) An entire specimen (not the one used in the study); (b) the specific specimen under investigation; (c) the detail of one spot on the weevil's exoskeleton. The scales are clearly apparent and display a range of colours. The scales of interest are in the orange zones.

*Electronic address: jean-pol.vigneron@fundp.ac.be

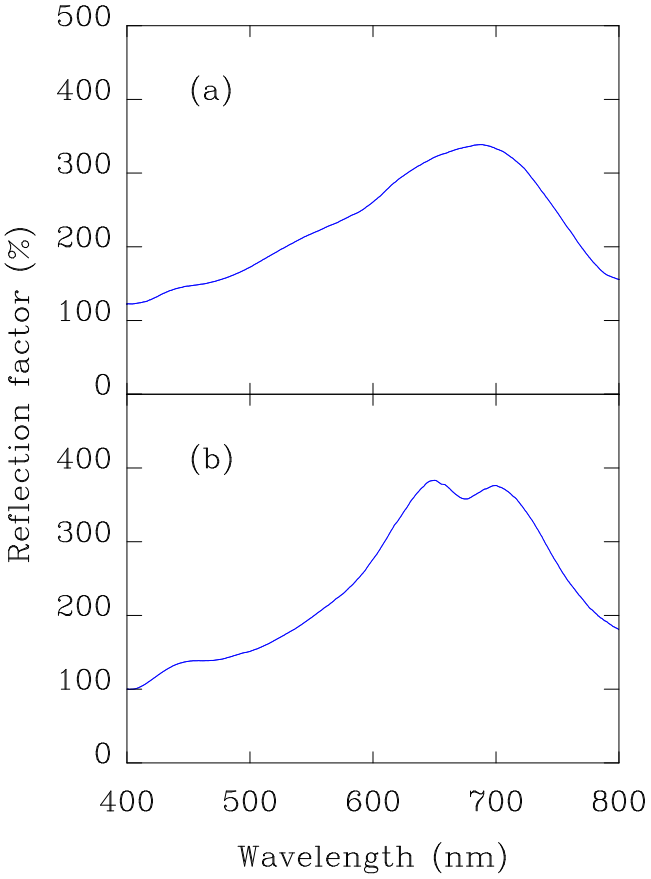

FIG. 2: (Colour online) The reflectance spectrum of some orange scales of the weevil *Pachyrrhynchus congestus pavonius*. The dominant wavelength can be located around 675 nm, but the reflection spectrum is rather broad, extending far into the red and yellow chromatic regions. The spectrum in part (a) has been obtained by illuminating and collecting the reflected light through the objective of a microscope. In this case, the incidence angle is not well defined, the uncertainty being estimated to be 58^o. This curve is also an average over several orange scales. Part (b) is the spectrum obtained by illuminating the sample with a high-intensity parallel beam and collecting the reflected light through the objective of a microscope. In this case, the incidence angle θ is well-defined, but cannot be set to zero, because of the volume occupied by the distinct source and collection probes (here, $\theta = 27^o$).

II. OBTAINING SAMPLES

Weevil samples were obtained from a commercial insect supplier, who identified them to sub-species level as *Pachyrrhynchus congestus pavonius*. This identification was checked by comparing the insects obtained with museum specimens and with descriptions in the literature [7].

III. REFLECTANCE FROM THE ORANGE SCALES

The normal-incidence specular reflectance from the orange scales was measured with an Avaspec 2048/2 optical-fibre spectrometer. The sample was placed on the sample-holder of an optical microscope and illuminated, through the microscope's lenses by the light from an halogen lamp. The reflected light was collected, again through the microscope's optics, by the aperture of an optical fibre, and diverted to the spectrophotometer. In this way, it was possible to conduct measurements on a specific single scale. The reflected light was compared with the light diffused by a white standard, which followed the same path in the optical microscope. The observed spectrum for the average of several scales is shown in Fig. 2(a). Though some variations exist from one scale to another, the dominant wavelength can be located at a very desaturated wavelengths region close to 675 nm, identified in a pink-orange region of the chromaticity diagram. The spectrum is always found to be broad. A very weak blue reflectance is also perceived, but this weak colouration is not associated with any significant visual effect.

Regarding the broadening, it should first be noticed that the numerical aperture of the microscope objective (chosen to fit for the examination of a single scale) is rather large (0.85), so that the illumination takes place within an angle close to $\Delta\theta \simeq 58°$. This is related to the need of light focussing when selecting a small area for analysis. With a rather large illuminating solid angle, we see that the incidence and emergence angles are loosely defined, and this may impact the reflectance spectral resolution. This, in particular, arises when the coloring structure uses multilayer interference as part of the physical light filtering mechanism, when the dominant reflected wavelength changes with the incidence angle. As an example (which will be useful later), if the spectral sensitivity shows up to be

$$\frac{\Delta\lambda}{\Delta\theta} \approx 2 \text{ nm/deg} \qquad (1)$$

we can expect, in the present configuration, a spectral broadening close to $\Delta\lambda = 120$ nm.

Part of this broadening can be eliminated by changing the illumination geometry, at the expense of not being able to carry out a true normal-incidence measurement. Fig. 2(b) shows the reflection factor resulting from the use of a nearly parallel high-intensity beam generated by a halogen optic-fiber illuminator, at an incidence of $\theta = 27^o$ (the smallest incidence compatible with the shape and volume of the illuminating and collecting probes). As before, the light was collected by the microscope, forming a real image of a single illuminated scale. The fiber-optic probe collects the light it only from a specific area (well under the size of the scale image) of this real image. The finite acceptance angle of the fiber-optic probe also limits the useful emergence angles (providing a further collimation on the reflected beam), so that the attempted

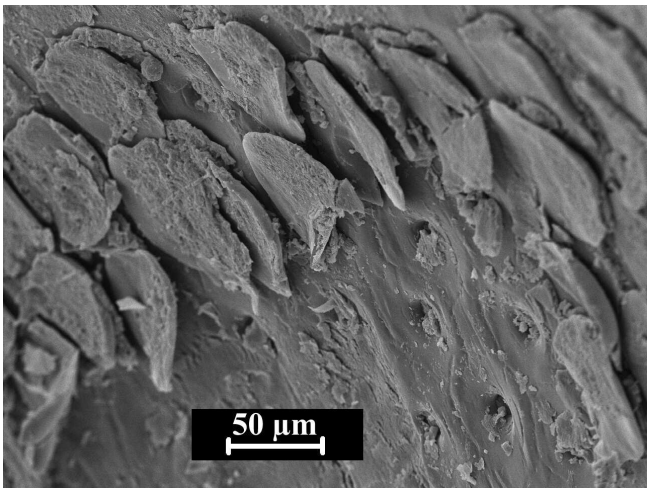

FIG. 3: Scanning electron microscope image of the weevil dorsal area, showing the scales and the scars left on the cuticle when the scales are removed.

interposition of a screen with a pinhole in front of the objective did not improve the resolution. It is clear from Fig. 2(b) that some bandwidth reduction is gained with this geometry, but also that the overall response function of the scale remains broad, producing a desaturated pink-orange colour.

Unexpectedly, the orange colour displayed on the weevil's rings is quite stable when the viewing angle is changed. This is already perceivable on images like those in Fig. 1(a) or Fig. 1(b), where, under a well-defined incidence, the coloured rings are visible, with the same colour, in spite of the fact that the normal to the cuticle surface, at the ring center, varies considerably from one ring to another. This suggests that the optical device, which produces the colouration, is not exactly an ideal photonic crystal, which would produce very sharp reflection bands which change dominant wavelength with the angle of incidence (see, for instance, ref. [8] or [9]). The optical properties shown here are, to some extent, better described as diffuse scattering than reflection or Bragg diffraction, though as will be seen below, it is explained by a photonic-crystal reflectance effect. The interpretation of these optical properties should account for the ultrastructure of the scales, as revealed, in the next section, by electron microscopy investigations, but also consider the avoidance of iridescence (the change of colour with viewing angle).

IV. SCANNING ELECTRON MICROSCOPY

The weevil cuticle is smooth on a large part of the body (the dark brown/black areas), but, as seen in Fig.3, the orange regions are covered with discernable scales. These scales are each attached to the exocuticle through a single pedicle and they can be easily removed individually. The small scar remaining after the removal of a scale can be seen in Fig. 3. The scale- length is of the order of 100 μm, the width, 50 μm, and the thickness, 5 μm.

Each scale is structured as shown in Fig. 4. The straight section normal to the scale's long axis shows a layered external "cortex" or "envelope" of chitin, which protects a very regular three-dimensional structure. The outermost side of this layered cortex (relative to the weevil) is somewhat less than 2 μm thick, whilst the innermost portion of the cortex (that between the weevil's body and the scale) is much thinner. The volume of the scale is filled with an extremely well ordered material, which can be viewed as a set of strongly corrugated sheets, parallel to the scale surface. This rigid structure is a three-dimensional periodic structure with two optical media : chitin and air. A typical length scale which describes the spatial organization of the structure is of the order of 300 nm, which suggests its importance for spectral filtering in the visible range.

The apparent periodic geometry shows that the material filling the scale volume is a photonic crystal. The air/chitin refractive index contrast is, of course, too small to generate omnidirectional band gaps but, in order to explain the reflectance, the important issue is to determine whether stop bands can be found in the visible range,

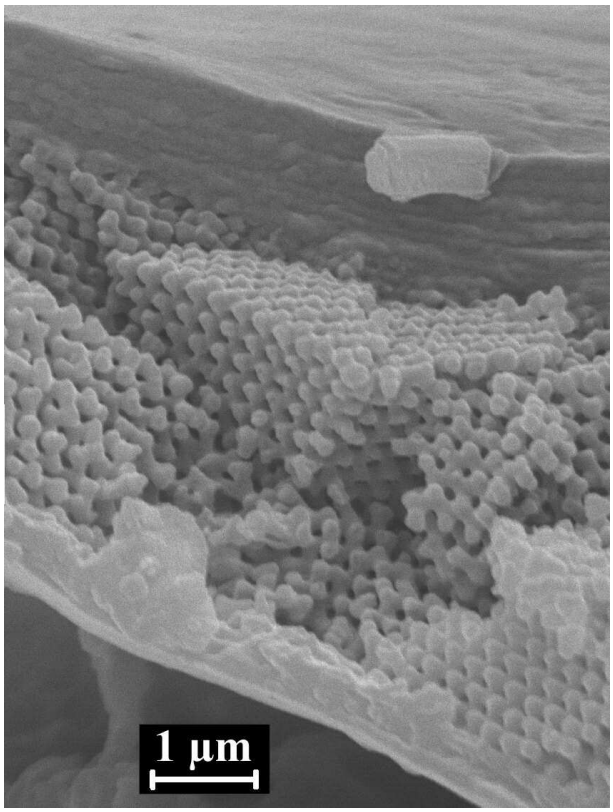

FIG. 4: Section of a scale normal to its surface and to its longitudinal axis. This SEM view shows the internal structure of the scales. The layered structure is apparent, but very regular fractures in the direction roughly normal to the layers indicate a highly correlated stacking of these layers.

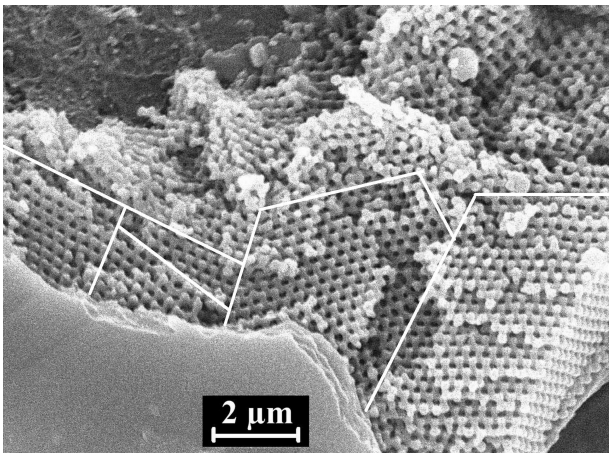

FIG. 5: Scanning electron microscope image of the internal structure of a scale, showing the layered organization. The layers appear to be made from a chitin sheet, perforated by a triangular lattice, with a unit cell containing one hole and one protrusion. Some long-range spatial incoherence is also observed, suggesting a superstructure with domains showing a variable orientation. This kind of structure is better described as a photonic polycrystal than as a photonic crystal.

contributing to a spectrally selective diffusion. The photonic crystal, as observed is not perfect: slight variation of the perforations diameter occur within a sheet, and the orientation of the lattice is not constant. Indeed, as seen on Fig. 5, domains with distinct orientations can be identified, and this adds to the complexity of the photonic structure. The modelling of such a structure calls for two stages : first, the identification of the reflectance of an ideal photonic-crystal structure with parameters exctracted from the SEM pictures, and, second, consider the effect brought by the polycrystalline superstructure on the optical properties.

V. LOCAL PHOTONIC-CRYSTAL

A. Geometric parameters

The electron microscope images (see Fig. 4 and Fig. 5) show a stack of perforated plates, which are arranged on top of each other in a geometrically coherent way. Though scanning-electron images each convey limited information, due to the two-dimensional presentation of the data, it is possible to assess the present structure rather accurately. The visible part of the structure, in Fig. 5, is the top-most layer, which appears as a thin plate of chitin, perforated by a series of circular holes, arranged along a two-dimensional triangular lattice. This single layer structure is idealized on Fig. 6, which shows the chitin plates, and a periodic array of cylindrical holes and protrusions. The distance between the centers of any two neighboring holes is $d = 333$ nm (± 3 nm), a value which can be rather precisely known from the electron microscope images, because of the mid-range coherence, and assuming a perfect hexagonal symmetry, which allows to estimate the surface normal deviation from the view axis, on the two-dimensional image. The radius of the holes can also be estimated to $h = 76$ nm from the images, though with less accuracy (± 8 nm). Protrusions show the same diameter, $b = 76$ nm.

The analysis of the possible stacking schemes which respect the structure symmetry (reported in appendix B at the end of the paper) shows that the corrugated plates are stacked in such a way that the resulting structure has a cubic symmetry. To this end, the protruding (A), flat (B) and empty sites (C) (see Fig. 7) must be aligned vertically, and repeated in that order ("ABC" stacking). The stacking distance between "A" and "B" layers, and between "B" and "C" layers must be $p = 272$ nm for a cubic structure, and this can be verified on some scanning electron images, confirming the structure symmetry. The protrusion height can be estimated by inspection of the scanning electron microscope images, and a value of 214 nm can be retained, leaving an average chitin plate thickness of 58 nm.

With these numbers, is relatively easy to determine the filling factor f of the crystal structure, i.e. the ratio between the volume occupied by chitin, and the total cell volume. The volume of the primitive cell, containing one hole and one protrusion, is easily evaluated to $21. \times 10^6$ nm^3, while the sum of the volume of the chitin sheet in the primitive cell, extended with the hemispherical protrusion, and reduced by the volume of the hole, gives a chitin volume per cell of 8.4×10^6 nm^3. This leads to a filling factor $f = 0.32$. The average value of the dielectric constant can then be estimated as

$$\langle \varepsilon \rangle = f\,(1.52)^2 + (1-f)\,(1)^2 = 1.42 \qquad (2)$$

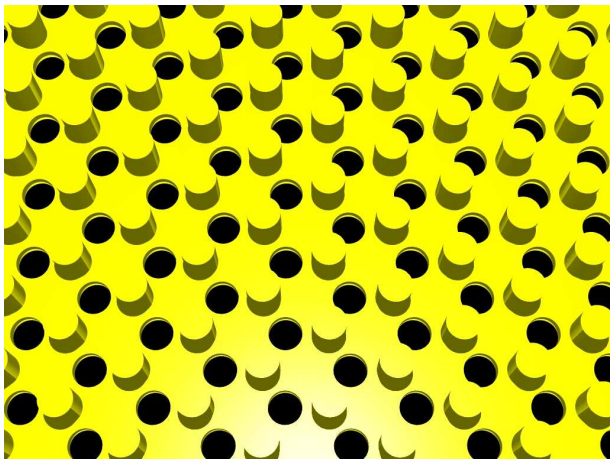

FIG. 6: (Colour online) Idealized structure of a chitin layer, which incorporates the geometry parameters deduced from an analysis of the SEM images.

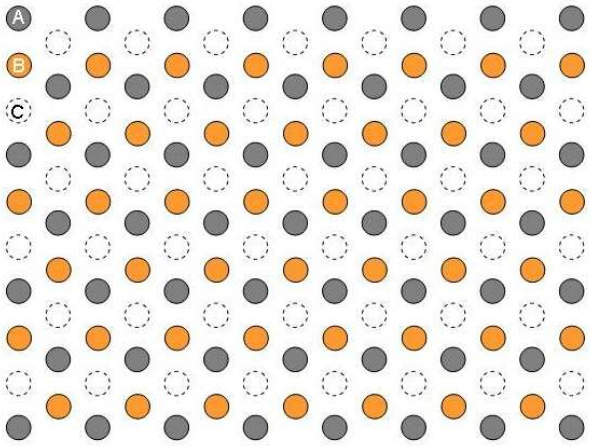

FIG. 7: (Colour online) The basic layer of the weevil scale structure is invariant under the translations of a triangular lattice. In the primitive cell, we find the elements for three coexisting sublattices : a sublattice of protrusions acting as spacers (A-sites), a sublattice of empty sites (B-sites), and a sublattice of holes (C-sites).

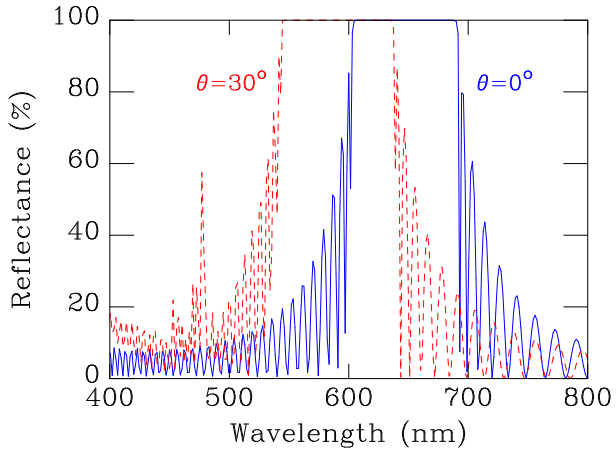

FIG. 8: (Colour online) Calculated reflectance of a stack of layers shown on Fig. 7, arranged to form a face-centered cubic lattice, for two angles of incidence, $\theta = 0°$ (normal incidence) and $\theta = 30°$.

or

$$\left\langle \frac{1}{\varepsilon} \right\rangle = f\frac{1}{(1.52)^2} + (1-f)\frac{1}{(1)^2} = \frac{1}{1.22} \qquad (3)$$

depending on the orientation of the surfaces with respect to the radiation electric field. Actually both averaging formulae lead to rather similar results, and the following estimation of the average refractive index for the whole photonic crystal should be reliable enough for our present purpose,

$$\bar{n} = 1.15. \qquad (4)$$

B. Dominant reflected wavelength

Before embarking on detailed numerical simulations of the reflectance of the layer structure described above, we can, at least for the case of normal incidence, determine the dominant reflected wavelength from such a photonic crystal. We take the point of view that the reflection occurs because of the presence of a photonic-crystal stop band, and we estimate the spectral location of this band by assuming an infinite repetition of the three-layers period shown in Fig. 7. We also assume weak refractive index differences and we average the structure in planes parallel to the layers: a procedure which, in principle, is only valid for incident wave sent close to normal incidence, when the wave periodicity parallel to the interfaces becomes much larger than the typical corrugation length along these directions. With all of these assumptions, reflection occurs at angular frequencies ω where a photonic gap occurs, i.e. when the average dispersion relation

$$\omega = k\frac{c}{\bar{n}} \qquad (5)$$

crosses a Brillouin zone boundary (where k is the norm of the wavevector in the averaged medium, and c is the light propagation speed in vacuum). This occurs at wavelengths λ such that

$$\lambda = \frac{2p\bar{n}}{m} \qquad (6)$$

where p is the multilayer periodicity (here, one-third of the real three-dimensional "ABC" periodicity, as the shifted layers are "smeared", and made equivalent, by lateral averaging), and m is an integer which brings the frequency in the range of interest (i.e., here, the visible spectral range). In a straightforward way, we obtain (with, as mentioned above, a period $p = 272$ nm)

$$\lambda = \frac{2 \times 272 \times 1.16}{1} = 626 \text{ nm} \qquad (7)$$

This wavelength is clearly in the orange-red part of the visible spectrum and compares well (for a broad band such as that observed here) with the dominant colour revealed by the measured spectra in Fig. 2. The structure just described then explains the dominance of an orange reflection from the scales in the annular markings of the weevil.

C. Ideal photonic-crystal reflectance spectrum

We can now proceed with a more complete investigation of the reflectance spectrum. The reflectance can be calculated from the geometry described in section V A if we completely ignore the superstructure of misoriented domains observed in Fig. 5 and idealize the structure to fit a perfect photonic-crystal film (thick enough to be considered "semi-infinite"). This computation uses a three-dimensional transfer-matrix technique [9, 10] and includes multiple-scattering effects at all orders. It is

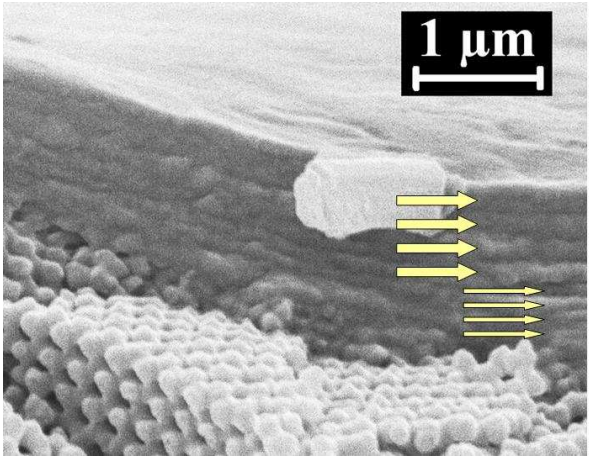

FIG. 9: Detail of the layered cortex which constitutes the outer part of a scale. This structure actually contains two distinct selective mirrors: the upper one reflects yellowish green light (peak wavelength 528 nm), while the one just below reflects purplish blue (peak wavelength 447 nm).

suitable for providing simulations of the specular and diffracted reflections as a function of the incident wavelength, the incidence angle, the azimuthal incidence angle, and the incident-wave polarization state. In Fig. 8, the reflectance spectrum is calculated for a stack of 16 three-layers periods, assuming a strict normal incidence, and using the geometric and optical parameters described above. The number of field harmonics used in the calculation was limited to 64, and only the transverse-electric (TE) incidence light was considered. The calculated reflectance spectrum turned out to be very simple : a sharp peak appears near 595 nm, in the orange spectral region. This is in good agreement with the dominant wavelength estimated in section V B, and with the maximum of the experimental spectrum (see Fig. 2). The spectral band is, however, much narrower than that of the experimental graph and , moreover, the spectral location of this narrow band changes with the incidence angle, which implies that we should see iridescence, i.e. a change of colour when viewing the surface under different angles. This iridescence, as was mentioned above, is not seen in the experimental analysis.

D. Polycrystal structure averaging effect

The above results from a perfect photonic crystal shows that if an ideal structure can crudely account for the orange coloration of the weevil's scales, it cannot explain the broad spectrum observed experimentally. Fig. 2(a) and 2(b) shows that, in the measurement, the numerical aperture tends to broaden the spectrum, but when the best effort is made for improving on this, there remains a spectral width which should be explained.

The scale of the weevil is not an infinite semi-crystal, as first assumed above. The material inside the scale cortex shows domains, and irregular interfaces between domains, which cause light diffusion. With multiple scattering, such diffused waves meets the reticular planes of the domain crystallites following many different incidence angles, so that even if the external incident wave is well defined, the internal incidence angles on the domains surfaces do not keep any memory of the external incidence angle [11]. This chaotic behavior can occur with even a very small number of crystallite interfaces inside the scale and has essentially two consequences : the first one is to decorrelate the emergent from the incident wave directions, so that the illuminated surface loses much of the metallic appearance expected from short-period three-dimensional photonic-crystal surfaces; in that situation, the colour can be viewed from any direction, irrespective of the illumination direction, as observed even with the naked eyes on the orange rings of the weevil. The second one is that the spectrum will be smeared out because for any external incidence, we will be able to find, in the multiply scattered beam, a range of internal incidences from which different wavelengths will be dominantly scattered.

We investigated this averaging effect by computing numerically a spectrum that contains, in a uniform way, all incidences (zenithal and azimuthal) on the surface of the photonic crystal with the structure described in section V A. The result is shown in Fig. 10, which describes the average reflectance for unpolarized incident light. This reflectance models the reflection factor measured and represented in Fig. 2. One immediately sees that, even if the calculation locates the reflection band at wavelengths slightly shorter than observed, the agreement is reasonable for both the dominant wavelength (and hence the predicted colour) and for the band width (and hence the

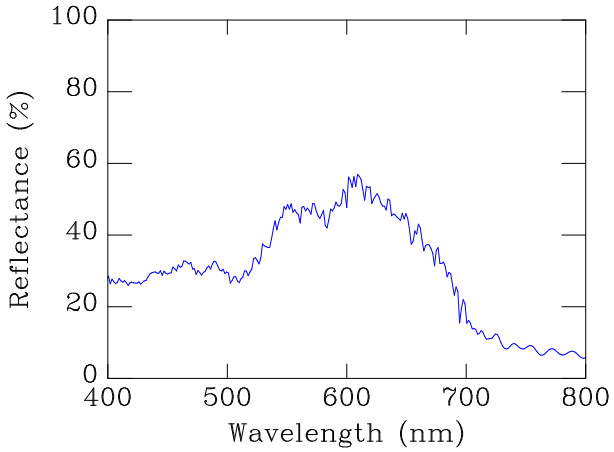

FIG. 10: Hemispherical reflectance of the ideal weevil scale photonic crystal, averaged over the incidences in the entire illumination hemisphere (zenithal and azimuthal angles). The experimental reflection factor reported on Fig. 2 is better modelled by such an average because of the chaotic scattering induced by the polycristalline nature of the photonic structure which produces the filtered reflection. This transfer-matrix calculation converged with 16 Fourier components.

desaturation). As in the experimental spectrum, the reflectance exhibits a double peak with distinctive components separated by about 50 nm.

This chaotic reflection, due to the presence of domains in the photonic material of the scales, means that the emerging light has lost the memory of the external incidence direction. The consequence is that, whatever the illumination setup, the orange coloration of the rings will be seen from everywhere. It also means that the colour filtering will not depend strongly on the illumination and viewing directions, though the building bloc of the polycrystal photonic structure *does* produce a strong iridescence.

Breaking iridescence with a polycrystal is not a completely new mechanism in nature. The Brazilian butterfly Cyanophrys remus, for instance (and probably many others) have been shown to use a photonic polycrystal on the scales of the ventral side of their wings to produce a non-iridescent pea-green cryptic coloration [12].

E. Side contributions

The face-centred cubic material only fills the interior of the scale: the external part is a cortex which is more than 1 μm thick and, as can be seen in Fig. 8, is actually formed by two types of layers. The four exterior-most layers, just below the surface of the scale, show a thickness of 176 nm. As the average refractive index of the cortex must be close to $\bar{n} = 1.5$ (a little less than the index of pure chitin), the dominant reflection wavelength must be

$$\lambda = 2 \times 176 \times 1.5 = 528 \text{ nm} \tag{8}$$

This is not visible on the experimental reflection, possibly because of the very small number of interfering waves in this very thin structure. It is interesting to note that the small bump just below 450 nm in the experimental reflectance could also be tentatively explained by the structure of the cortex : the deeper layers, in contact with the inverse-opal-like filling, have a thickness of 149 nm, from SEM observation. The reflection wavelength associated with these layers can be calculated as before :

$$\lambda = 2 \times 149 \times 1.5 = 447 \text{ nm} \tag{9}$$

and this coincides with the purplish-blue bump. If this is true, we have, in *Pachyrrhynchus congestus pavonius* a three-component dielectric mirror, but contrasting other broadband mirrors which make use of stacked one-dimensional multilayers[13], the present one combines two multilayers and a special, three-dimensional polycrystal. This very evolved structure is probably worth further study, and the investigations should probably not be limited to the mechanisms of optical reflection.

VI. CONCLUSION

In this work, we have shown the orange colouration of the weevil *Pachyrrhynchus congestus pavonius* to be associated with the three-dimensional structure which fills the scales of the coloured rings. The crystal structure has been identified as a photonic polycrystal, the crystallites (or domains) being organized as a face-centred cubic crystal. this structure developes as a stack of layers invariant under the translations of a triangular lattice. A two-stages model was developed, which idealizes the observed geometry. This model complies with the data that was measured from the SEM images and assumes a cubic symmetry. The first stage of the model idealizes the structure as a coherent photonic-crystal film, infinite in the lateral directions. This leads to narrow reflections bands which shift to shorter wavelengths with increasing incidence angles. If the order of magnitude of the reflection wavelengths is acceptable, the sharpness of the reflection bands and the iridescence contradict experiment and naked eyes observation. The second stage of the model repairs these paradoxical results by accounting for internal scattering due to the presence of cristal domains varying in orientations, and separated by diffusive interfaces. The presence of these defects leads to isotropic scattering which strongly decorrelates the incident and emergent light beams. This loss of memory of the beam orientation explains both the diffuse scattering produced by the photonic structure and the broad spectrum actually observed.

The colouration of this genus of weevils is among the most astonishing visual effects displayed in nature. Many animal species which are distasteful to predators have evolved aposematism (they have a distinctive, conspicuous colouration, which functions as a warning signal, advertising their inedibility to potential predators). Wallace notes in a passage on the genus *Pachyrrhynchus* (see p 292 of [14]) that many weevils have excessively hard integuments, which render them inedible to most birds and our own dissections of this species confirm their extremely tough exoskeleton. It seems likely, therefore, that the stark colouration of this species is a form of aposematism. Further evidence in support of this comes from the finding that a number of edible species, such as the longicorn beetles *Doliops curculionides* and *Doliops geometrica* and the cricket *Scepastus pachyrhynchoides* mimic various *Pachyrrhynchus* species weevils [14].

APPENDIX A : INCIDENCE ANGLE DEFINITION IN MICRO-REFLECTANCE MEASUREMENTS

As discussed in the text, a microspectrophotometer can be used to measure the reflectance from small areas, which is important here, as the scales of the weevil (about 50 μm in diameter) occupy just thin circular stripes on the weevil cuticle. The instrument is basically a micro-

scope which is able to provide illumination focussed on the object, through the objective. The scattered light returns to the objective and converges back to forms an image, a small portion (pixel) of which is sent to the spectrophotometer. The conditions for the measurement are restrictive : long-focal objectives define the incidence angle pretty well, but form an image of low magnification, which is not suitable for spectral analysis of a point-like object. Short-focal objectives provide higher magnifications but the numerical aperture is larger and the incidence angle is less well defined. When the reflectance bands shift with varying incidences, the uncertainty on the incidence angle can limit the spectral resolution of the measurement. Restriction of the acceptance angle of the objective by a diaphragm can improve the situation, but reduces the intensity to be measured.

In the present work, the measurement could be improved by first using an external illuminator (150 W) providing a nearly parallel incident beam (10^o divergence) and collecting the light through a diaphragm and the objective of a microscope, collecting the light by an optic-fiber probe in the image plane of the microscope. In this arrangement, the optics fiber, which has a numerical aperture of N.A.=0.22, provides a collimating effect, so that the measurement is not drastically altered by closing the diaphragm.

APPENDIX B : SYMMETRY OF THE THREE-DIMENSIONAL PHOTONIC-CRYSTAL STRUCTURE IN THE WEEVIL'S SCALE

In this appendix, we give more details on the analysis of the SEM images, leading to the conclusion that the layered slabs of triangular symmetry can be stacked to form a photonic crystal structure with a face-centered cubic lattice.

On the perforated and bumpy slabs revealed by SEM (see section IV, each hole has six nearest neighbours, and lies at the centre of a regular hexagon formed by these neighbours. The distance between the centres of any two neighbouring holes is, as mentionned above, $d = 333$ nm, from centre to centre. The triangular lattice of holes leaves two, inequivalent, other sites with the full triangular symmetry. One of them is occupied by a protrusion with a shape between hemispherical and cylindrical. It is somewhat more difficult to assess the diameter of the protrusions, but since the distance between neighbouring triangular site in this crystal structure is $d/\sqrt{3}$, the space left for the protrusion base limits its radius to $b < 116$ nm. Inspection of the SEM images indicates that, in fact, the protrusion diameter is of the same order as the diameter of the holes, so that we can model the structure with $b = h = 76$ nm. On the SEM views, these protruding spacers are apparent in Fig. 5, from an appropriate perspective, and less visible under a strict normal observation. The cylindrical spacers are distributed on a triangular lattice similar to the lattice of holes, except for a constant translation of length $d/\sqrt{3}$. This translation brings them at equal distances from their three neighbouring holes. The third triangular site, not occupied by a hole or a protrusion is empty and simply leaves a view of the chitin sheet.

The corrugated and perforated slabs are stacked on top of each other in a direction normal to the surface of the scale, in such a way that each perforated slab runs parallel to the surface of the scale. The stacking of such an hexagonal structure, while keeping all C_{3v}-symmetry sites (those sites where 120° vertical-axis rotations leave the structure invariant), can be obtained in just three different ways, and the examination of the SEM pictures helps with choosing the correct one. In the next discussion, we will name the three C_{3v}-symmetry sites in the following way (see Fig. 6) : the A-site is the protrusion-centre location, the B-site is the empty C_{3v} site, and the C-site is the hole-centre location. The stacking options are then not so numerous. On top of the protrusion, we can either have an A-site, a B-site, or a C-site. Starting with the A-site, and then again, would mean an "AAA..." stacking, where the holes would form a rectilinear free channel, which is not observed. The "ACAC..." stacking would force the matching of a protrusion with a hole, which is mechanically awkward and is not observed either. The "AB " stacking assumes the contact of the protrusion with the chitin plate at the empty site, and implies another move of the third layer, which brings the C-site over the empty B-site. The stacking is then actually of the type "ABCABC...". The shift of each successive layers is, in this model, 192 nm, in good agreement with the observations. This oblique alignment of the layers can be seen, for instance in SEM pictures such as that in Fig. 4. We note that the "AAA..." stacking would give rise to the simple hexagonal lattice, the "ABAB..." stacking would lead to the hexagonal compact lattice, while the "ABCABC... " stacking leads to the face-centred cubic lattice, if the distance between the layers matches the appropriate symmetry requirement. Fractures containing the normal to the layers exist on the prepared samples, and on these faces, an hexagonal structure also reveals itself. Furthermore, no compression of the hexagonal cells is perceived, so that the exact face-centred cubic structure can be assumed. In such a structure, the distance between A and B layers, and the distance between B and C layers are given by $p = a/\sqrt{3}$, where $a = d\sqrt{2} = 471$ nm, which means $p = 272$ nm. The protrusion height can be estimated from inspection of the SEM images, and a value of 214 nm can be retained. This leaves a chitin plate thickness of 58 nm. This is a rather thin plate, but this simply means that the basic scatterers in this structure are the roughly cylindrical "spacers". In three dimensions, these scatterers are distributed on a face-centred cubic lattice. The structure can then be called an "opal" or an "inverse opal" (even if we recognize that the structure is not exactly an assembly of spheres), according to the filling factor of the structure (the ratio of the chitin volume per cell to the complete cell volume).

More chitin than air defines the "opal", while more air than chitin should rather define the "inverse opal".

Acknowledgments

We wish to thank Darren Mann of Oxford University Museum of Natural History and Max Barclay of the Natural History Museum in London for facilitating access to these museums' collections and to Darren Mann additionally for assistance tracing some of the literature on the genus *Pachyrrhynchus*. This work was carried out with support from EU5 Centre of Excellence ICAI-CT-2000-70029 and from the Inter-University Attraction Pole (IUAP P5/1) on "Quantum-size effects in nanostructured materials" of the Belgian Office for Scientific, Technical, and Cultural Affairs. The authors acknowledge the use of Namur Interuniversity Scientific Computing Facility (Namur-ISCF), a common project between the Belgian National Fund for Scientific Research (FNRS), and the Facultés Universitaires Notre-Dame de la Paix (FUNDP). This work has also been partly supported by the European Regional Development Fund (ERDF) and the Walloon Regional Government under the "PREMIO" INTERREG IIIa project. The work was also supported in part by EU6 BIOPHOT/NEST grant. V.L. was supported as postdoctoral fellow by the Belgian National Fund for Scientific Research (FNRS). V.W. was supported for part of this work by a Fellowship from The Royal Commission for the Exhibition of 1851.

[1] A. R. Wallace, British Association for the Advancement of Science Report **46**, 100 (1876).
[2] A. R. Parker, V. L. Welch, D. Driver, and N. Martini, Nature **426**, 786 (2003).
[3] S. Berthier, *Iridescences, les couleurs physiques des insectes* (Springer-Verlag, Paris, 2003).
[4] H. Ghiradella, Ann. Entomol. Soc. Am. **77**, 637 (1984).
[5] V. L. Welch, *in Structural colours in Biological Systems-Principles and Applications* (Osaka University Press, Osaka, 2005), edited by S. Kinoshita and S. Yoshioka.
[6] A. R. Parker, Recent Research in Developmental Entomology **5**, In Press (2006).
[7] W. Schultze, Philip. Journ. Sci. **24**, 309 (1924).
[8] J. P. Vigneron, M. Rassart, C. Vandenbem, V. Lousse, O. Deparis, L. P. Biró, D. Dedouaire, A. Cornet, and P. Defrance, Phys. Rev. E **73**, 041905 (2006).
[9] J. Vigneron and V. Lousse, Proc. SPIE **6128**, 61281G (2006).
[10] J. B. Pendry and A. MacKinnon, Phys. Rev. Letters **69**, 2772 (1992).
[11] J. Schroeder and J. H. Rosolowski, in *Emerging Optical Materials, SPIE Proceedings Volume 297. Edited by Solomon Musikant. Bellingham, WA: Society for Photo-Optical Instrumentation Engineers*, edited by S. Musikant (1981), p. 156.
[12] K. Kertész, Z. Bálint, Z. Vértesy, G. I. Márk, V. Lousse, J. P. Vigneron, M. Rassart, and L. P. Biró, Phys. Rev. E **74**, 021922 (2006).
[13] A. R. Parker, D. R. M. Kenzie, and M. C. J. Large, J. Experimental Biology **201**, 1307 (1998).
[14] A. R. Wallace, *in Science for All*, vol. 2 (Cassell, Petter, Galpin and Co., London, Paris and New York, 1879), edited by R. Brown.